

See discussions, stats, and author profiles for this publication at: <https://www.researchgate.net/publication/257949225>

Tribological properties of nanocrystalline diamond films deposited by hot filament chemical vapor deposition

Article in *AIP Advances* · August 2012

DOI: 10.1063/1.4751272

CITATIONS

22

READS

909

8 authors, including:



Kalpataru Panda

Universität der Bundeswehr München

58 PUBLICATIONS 1,263 CITATIONS

[SEE PROFILE](#)



Sonali Dash

Chandigarh University

218 PUBLICATIONS 2,960 CITATIONS

[SEE PROFILE](#)



Cyril Popov

Universität Kassel

182 PUBLICATIONS 2,279 CITATIONS

[SEE PROFILE](#)

Some of the authors of this publication are also working on these related projects:



the socio political system of the goemai [View project](#)



Studies on Hampi Musical Pillars [View project](#)

Tribological properties of nanocrystalline diamond films deposited by hot filament chemical vapor deposition

N. Kumar, K. Panda, S. Dash, C. Popov, J. P. Reithmaier et al.

Citation: *AIP Advances* 2, 032164 (2012); doi: 10.1063/1.4751272

View online: <http://dx.doi.org/10.1063/1.4751272>

View Table of Contents: <http://aipadvances.aip.org/resource/1/AAIDBI/v2/i3>

Published by the AIP Publishing LLC.

Additional information on AIP Advances

Journal Homepage: <http://aipadvances.aip.org>

Journal Information: <http://aipadvances.aip.org/about/journal>

Top downloads: http://aipadvances.aip.org/features/most_downloaded

Information for Authors: <http://aipadvances.aip.org/authors>

ADVERTISEMENT



Goodfellow

metals • ceramics • polymers
composites • compounds • glasses

Save 5% • Buy online
70,000 products • Fast shipping

Tribological properties of nanocrystalline diamond films deposited by hot filament chemical vapor deposition

N. Kumar,^{1,a} K. Panda,¹ S. Dash,¹ C. Popov,² J. P. Reithmaier,²
B. K. Panigrahi,¹ A. K. Tyagi,¹ and Baldev Raj¹

¹Indira Gandhi Centre for Atomic Research, Kalpakkam 603 102, TN, India

²Institute of Nanostructure Technologies and Analytics, University of Kassel, Germany

(Received 1 May 2012; accepted 23 August 2012; published online 30 August 2012)

The dependence of the structural and morphological properties of nanocrystalline diamond films grown by hot filament chemical vapor deposition on the substrate temperature was studied. Friction coefficients of these films were measured and found to vary from high to ultra low, depending on the chemical nature of the films i.e., sp^2 and sp^3 phase fractions. For all films, the friction coefficient was found to decrease with increase in sp^2/sp^3 phase fraction. The wear rate follows the trend of the friction coefficient and was likewise found to depend on the structural and morphological properties of the films. For all the films, the friction coefficient is found to decrease with normal load which is ascribed to sliding induced surface amorphization/graphitization. Copyright 2012 Author(s). This article is distributed under a Creative Commons Attribution 3.0 Unported License. [<http://dx.doi.org/10.1063/1.4751272>]

I. INTRODUCTION

Diamond is known to be one of the stiffest and hardest of all known materials.¹⁻³ It has high elastic modulus, high fracture toughness, high thermal conductivity, low thermal expansion coefficient and high chemical inertness. This superhard material depicts broad optical transparency, high refractive index, wide band gap and negative electron affinity.^{4,5} These unique and exceptional qualities make diamond ideal for several industrial applications such as wear resistant coatings which are the most promising.⁶⁻⁸ Nanocrystalline diamond (NCD) films exhibit unique tribological properties due to their nanosized grains with increased ratio of surface to volume atoms resulting in distinct physical and chemical properties as compared to the bulk diamond.^{9,10} Nevertheless, the friction and wear of nanocrystalline diamond are quite anisotropic and depends on various factors, such as the chemical reactivity of the surface, crystallite size, crystallographic orientation, existence of dangling covalent bonds, sliding direction of oriented planes, surface roughness, properties of transfer layers, test environment and finally test parameters which influence the wear behavior, such as load and sliding velocity.^{8,11-15} In addition to all known important factors and tribological test parameters which may influence the wear behavior of the NCD films, the amount of hydrogen and sp^3/sp^2 bonding ratio play a dominant role in the friction and wear performances of these materials.¹⁶ There are several physical and chemical methods to synthesize NCD films. The hot filament chemical vapor deposition (HFCVD) technique is one of the most common methods due to its low cost; it allows the diamond deposition in a simple way as compared to more sophisticated plasma CVD techniques.¹⁷

The aim of the present paper is to investigate the tribological properties of NCD films with varying sp^2/sp^3 phase fractions. The friction and wear behavior was studied as a function of the applied normal load. Chemical behavior of the film surface, wear track and ball counterbody were used to explain the friction and wear behavior.

^aCorresponding author: N. Kumar, Phone/Fax: +914427480081, E-mail: niranjan@igcar.gov.in



II. EXPERIMENTAL

The diamond films under investigation were synthesized by hot filament chemical vapor deposition (HFCVD) from CH₄/H₂ mixtures with 1% methane. Silicon wafers were ultrasonically pretreated for 1 hour prior to the deposition in a suspension of 80 mg ultradisperse diamond powder (3–5 nm grain size) and 50 mg nanocrystalline diamond powder (250 nm average grain size) in 75 ml n-pentane in order to achieve a nucleation density of $1 \times 10^{10} \text{ cm}^{-2}$.¹⁸ During the deposition, the only parameter varied was the substrate temperature. It was 870°C for sample F1, 700°C for F2 and 600°C for F3. The other process parameters were kept constant. The working pressure was 25 mbar and gas phase composition of 1% CH₄ in H₂ was used during the film growth process. The deposition duration of all films was 180 minutes. The chemical bonding states were investigated by X-ray photoelectron spectroscopy (XPS) using a SPECS photoelectron spectrometer with monochromatic Al K α radiation at 1486.74 eV with an energy resolution of 0.6 eV. The spectrometer was calibrated before the measurements to the ISO standard. Two XPS spectra were taken on each sample at random locations and they were found to be rather similar at each location. Scanning tunnelling microscopy (STM) measurements were carried out using a commercial UHV–STM (150 Aarhus, SPECS GmbH) operating at a base pressure of 10^{-10} mbar. Tunnelling tips were prepared by electrochemical etching of tungsten wires of 0.3 mm diameter. Imaging was carried out with a set current of 0.7 nA and with a relatively high bias voltage between –5.0 to +5.0 V. The scanning tunnelling spectroscopy (STS) spectra were obtained during the scanning and the data presented here are the average of 10 reproducible spectra acquired during subsequent scans. Current imaging tunnelling spectroscopy (CITS) in STS mode was carried out to map the surface conductivity of all films.

Nanoindentation measurements (CSM Instruments, Switzerland) were performed with a diamond Berkovich indenter with a loading-unloading rate of 4 mN/min up to a maximum load of 10 mN. The method of Oliver and Pharr was applied to calculate the elastic modulus and hardness of the coatings.¹⁹ A ball-on-disk micro-tribometer (CSM Instruments, Switzerland) working in linear reciprocating mode was used for the tribological tests. A spherical steel ball (100Cr6 SS) of 6 mm diameter with a surface roughness of 0.06 μm was used as a sliding counterbody to measure the friction coefficient at three different normal loads of 1, 3 and 6 N at constant sliding speed of 1.5 cm/s. A test stroke length of 3 mm was used. The total sliding distance for each measurement was 10 m. The friction test was conducted in ambient atmospheric (dry and unlubricated) condition at room temperature. The relative humidity of the ambient atmosphere during the test was 58%. The wear rate k was calculated from the relation $k = V/(F \times S)$, where F , S and V are the normal load, the sliding distance and the wear volume, respectively. To obtain the wear volume, the wear depths were measured *in situ* with a linear variable differential transformer (LVDT) sensor coupled with the tribometer while the wear widths and lengths were determined with an optical microscope. The measurements were repeated five times on each sample and the results were found to be reproducible. The deviations represented by the error bars are given in the respective figures. The roughness of the film surface and the wear track was measured by “NanoMap 500LS” in a contact mode. The roughness in the wear track is determined along the track length. The diamond tip radius was 5 μm and the profiling was carried out at a load of 5 mg in ambient conditions. Three measurements on different locations of the film surface and wear track were carried out. In this case, the standard deviations were also calculated and the error bars are given in the following figure. Raman spectra on the surface of as-deposited films and inside the wear tracks were recorded in back scattering geometry using the 325 nm line of a helium-neon laser of Renishaw micro-Raman spectrometer (Model INVIA).

III. RESULTS AND DISCUSSION

Morphology and corresponding cross-sectional images of the nanocrystalline diamond films are shown in Figure 1 and Figure 2, respectively. At the highest substrate temperature of 870°C, larger grains with diameters of ≈ 100 nm are obtained while the film thickness is 0.6 μm [Figure 1(F1), Figure 2(F1)]. However, by decreasing the substrate temperature to 700°C and 600°C,

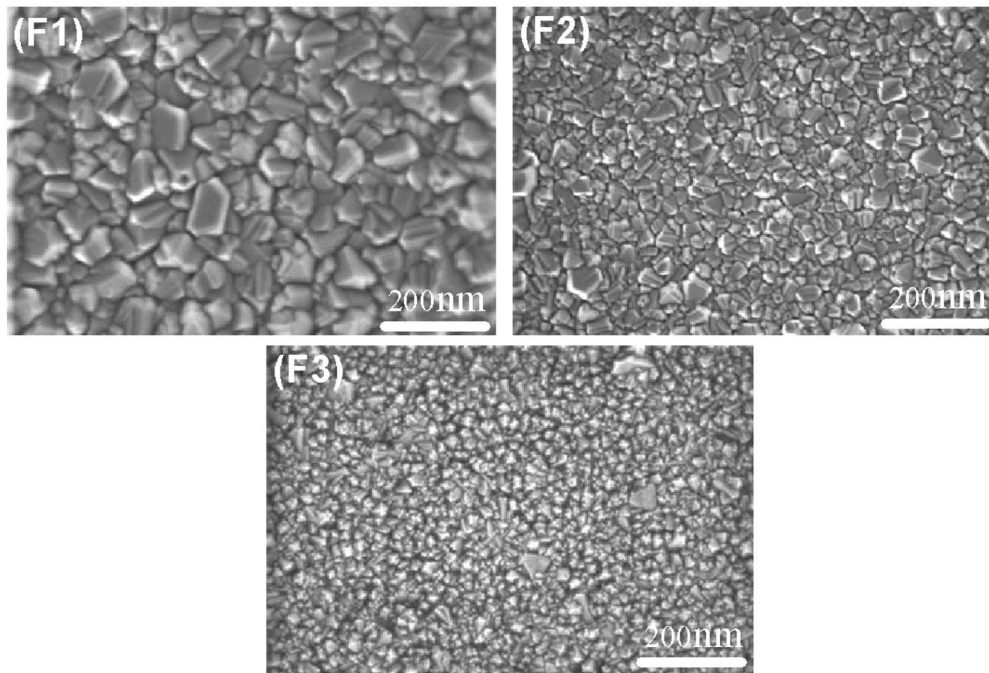


FIG. 1. Surface morphology revealed by FESEM images of films F1 (870°C), F2 (700°C) and F3 (600°C) films.

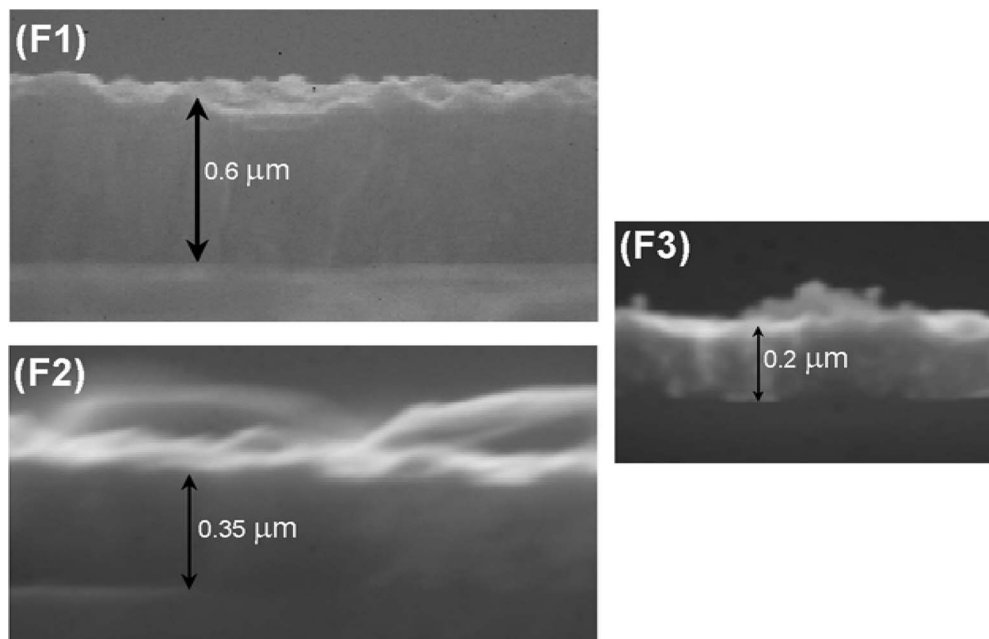


FIG. 2. Cross-section FESEM images of films F1 (870°C), F2 (700°C) and F3 (600°C).

respectively, both grain size and film thickness decreases [Figure 1(F2), Figure 1(F3)] and [Figure 2(F2), Figure 2(F3)]. The latter is a consequence of the fact that diamond growth is thermally activated.^{20–22} The microstructural properties of the films are summarized in Table I. Load-displacement curves during the nanoindentations were obtained at peak load of 10 mN as presented in Figure 3. Plastic energy is found to be minimum for film F1, however it is maximum

TABLE I. Physical and morphological description of diamond films.

No.	T_{sub} [$^{\circ}\text{C}$]	d (μm)	Grain size (nm)	H (GPa)	E (GPa)
(F1)	870	0.6	80–100	36.2	492.8
(F2)	700	0.35	50–70	32.6	432.3
(F3)	600	0.2	30–40	28.4	368.6

T_{sub} - substrate temperature, d - film thickness, H- hardness, E- elastic modulus.

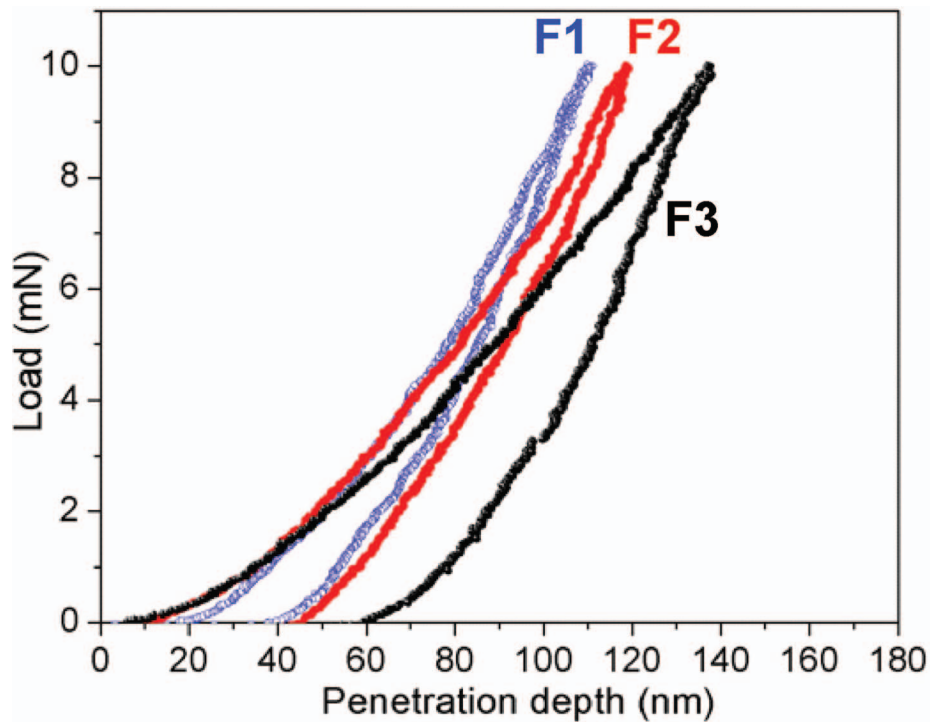


FIG. 3. Load-displacement curves of nanoindentations of films F1 (870 $^{\circ}\text{C}$), F2 (700 $^{\circ}\text{C}$) and F3 (600 $^{\circ}\text{C}$).

for F3. This behavior indicates high yield elastic stress with low plastic strain in film F1. The elastic recovery of the films changes in the order F3 (68%) > F2 (61%) > F1 (56%).

The core level C1s XPS spectra of the films are presented in Figure 4. The background of each spectrum was subtracted using Shirley's method.²³ The data were best fitted with Lorentzian peaks maintaining the FWHM constant during the fitting procedure and recording the peak binding energy shift. Chemical nature of the films significantly changes with the substrate temperature. The spectra show well defined peaks of $\text{sp}^2\text{C-C}$ and $\text{sp}^3\text{C-C}$ bonded carbon. The overall intensity of carbon related peaks is higher in films F2 and F3 comparing to F1. From the SEM images in Figure 1, it is seen that the diamond grain size is smaller for low substrate temperature growth conditions. Thus the amount of grain boundary volume fraction increases at lower temperatures. It can therefore be concluded that the sp^2 carbon is situated in the grain boundaries, which explains the higher sp^2 content in F2 and especially in film F3. It is evident from XPS that the phase fraction of sp^2 bonding increases with the smaller crystallite size. The increase of the crystalline quality with temperature up to ca. 950 $^{\circ}\text{C}$ is a well-known fact in diamond technology.^{4,5} For all three samples there is a shallow peak corresponding to C-O-C which stems from surface oxygen species. This oxygen surface contamination is not prominent as revealed by the intensity and area of these peaks as well by the low determined oxygen content of few at%. It is due to interaction of free dangling σ -bonds on the surface with O-containing species from the environment and varies slightly for the samples studied.

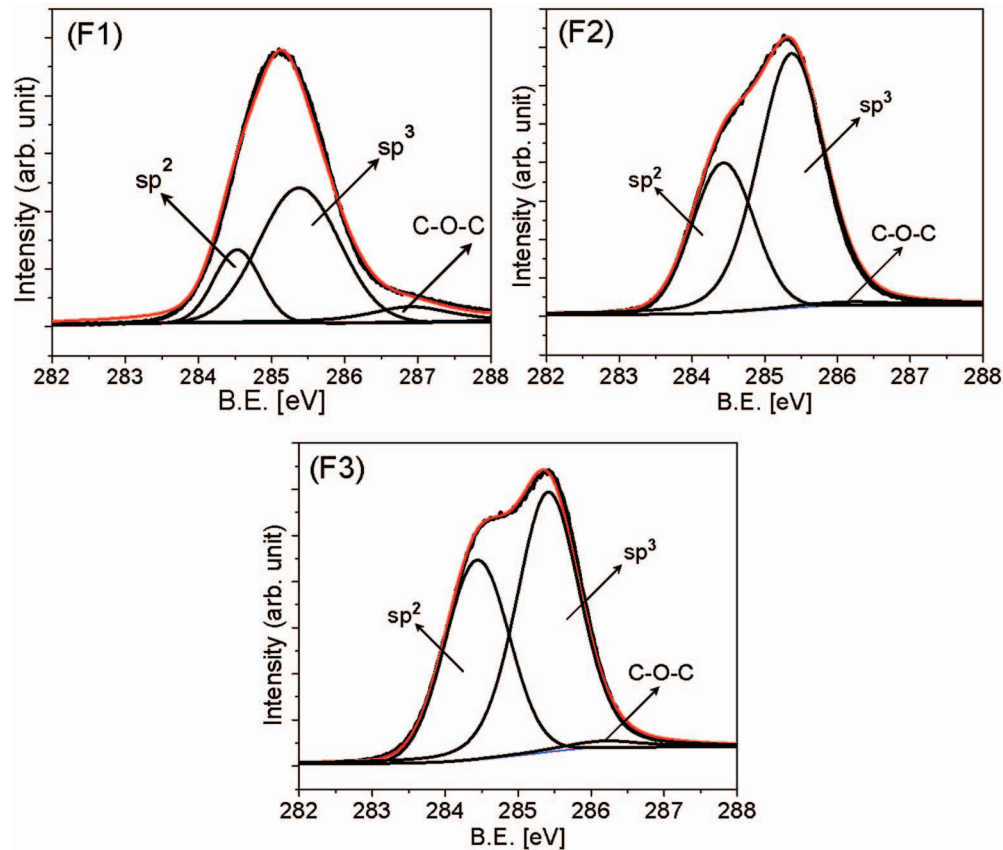


FIG. 4. XPS C 1s core-level spectra of films F1 (870°C), F2 (700°C) and F3 (600°C).

Surface electrical properties of the films under investigation were measured by STM. These measurements were not possible on as-prepared samples due to highly electrical resistive nature of the films. The surface of the films became conducting when sputtered with Ar^+ ion (5 kV) for one minute by removing ~ 1 nm thickness of the upper subsurface. Tunneling current versus sample voltage (I - V) spectra shown in Figure 5 is the average of 10 reproducible curves obtained on each film surface at different positions. Conductivity is found to enhance from micro to nanocrystalline (F1 to F3) diamond films. For input sample voltage of 1.5 V, film F1 shows a lower tunneling current of 0.06 nA in comparison to F2 (4.98 nA) and F3 (23.25 nA). The STM and the corresponding CITS images of films F1, F2 and F3, which represent the surface local conductivity are shown in Figure 6. The bright spots in CITS images correspond to conducting sites which emit electrons, while the dark spots belong to less conducting and almost non-emitting sites. The bright spots appear at the boundaries of the diamond grains in all three films and their density increases from film F1 to film F3. A higher density of the bright sites signifies that the film contains more amorphous carbon and graphite-like sp^2 phase at the grain boundary region. Typical I - V curves obtained from different grains 'g' and grain boundaries 'gb' of the film F3 (marked by arrows in Figure 6) are shown in Figure 7. It can be clearly seen that the grain boundaries have higher conductivity as compared with the grains. This clarifies the enhancement in conductivity of low temperature deposited films where the grains are smaller and the volume fraction of the grain boundary material, containing sp^2 bonded carbon atoms, is larger. The increase of sp^2 bonding from F1 to F3 is also studied by XPS and well correlated with STM and CITS analysis. The increase of conductivity of films with increasing sp^2 bonding fraction is also studied by Panda *et al.*²⁴

The variation of the friction coefficients of films F1, F2 and F3 with the sliding distance and the normal load are presented in Figure 8 and Figure 9(a), respectively, while the wear rates are given in Figure 9(b). The friction coefficients plotted in Figure 9(a) are the steady state friction values

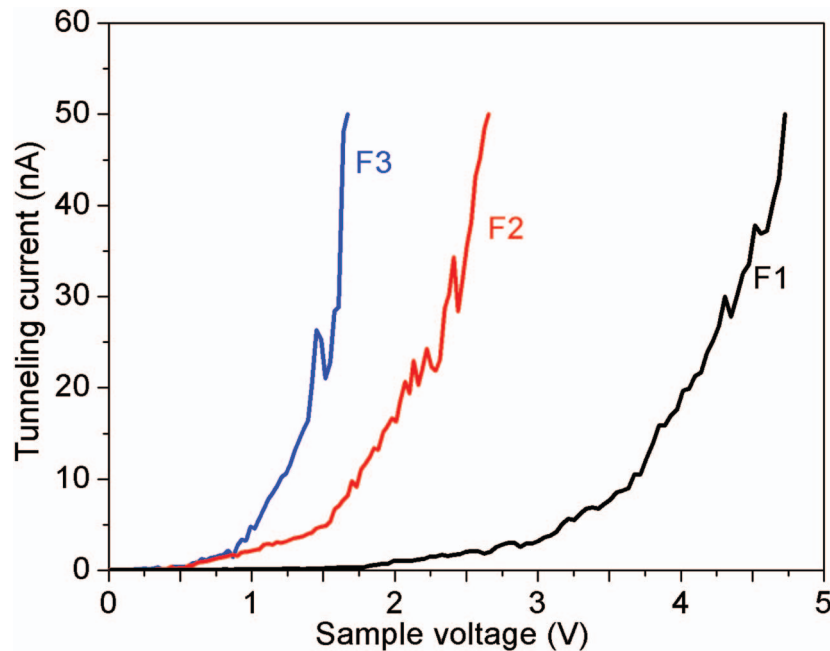


FIG. 5. I-V measurements of films F1, F2 and F3.

of Figure 8 with the respective deviations. Table II summarizes the whole information about the friction coefficients and the wear rates vs. the normal loads. The friction coefficient was found to decrease from F1 to F3 films as shown in Figures 8 and 9(a). The microstructure as well as hardness and elastic modulus of a material are known as one of the important factors influencing the friction and wear. The hardness and the elastic modulus increase with increasing the deposition temperature and respectively the grain size, as presented in Table I. Conventionally, high hardness, high elastic modulus and small grain size are all known factors to reduce the friction coefficient and wear rate of diamond films.²⁰ However, high friction coefficient is found for films F1, while low and ultra low friction coefficients are measured for films F2 and F3, respectively. For each specimen the wear rate is proportional to the normal load and this value decreases from F1 to F3. The film surface roughness and the wear track roughness were found to be nearly the same for all films F1, F2 and F3, as shown in Figure 10. The similar profiles of surface roughness on the diamond films and in the wear tracks indicate the formation of smooth wear track and possibly have no significant roughness effect on the friction coefficient. The stability of the friction curves (Figure 8) is an indication of smooth wear tracks inscribed during the tribo-tests.

Furthermore, low friction is directly related to the amorphization/graphitization of diamond near the sliding contact point.^{13,16} In one of the study it is seen that when diamond is polished, it undergoes sp^3 to sp^2 transition resulting in an amorphous adlayer that depends on surface orientation and sliding direction. The structural phase transformation and amorphization influence the change in friction and wear.¹³ To proof amorphization/graphitization of diamond films, Raman spectra were recorded on the film surface and in the wear track formed at 3 N load for each sample, as shown in Figure 11. All spectra have the following peaks in common: i) substrate-related silicon peaks at 520 cm^{-1} and $944\text{--}948\text{ cm}^{-1}$; ii) the fundamental diamond line (D^*) at about 1332 cm^{-1} stemming from crystalline diamond; iii) the known graphite-related G and D bands at $1573\text{--}1598\text{ cm}^{-1}$ and 1350 cm^{-1} and (iv) peaks at 1168 cm^{-1} and 1470 cm^{-1} corresponding to the formation of transpolyacetylene (TPA) segment, which are only observed for nano- and ultrananocrystalline diamond.^{5,22} It is evident from the spectra shown in Figure 11 that the intensity of the graphitic bands relative to the fundamental diamond line increases from F1 to F3 on the surface as well as in the wear tracks. A shift of the G band towards higher or lower frequency range describes stress or strain in the film, respectively.¹⁴ The relative intensity of the G band in the wear track decreases as compared

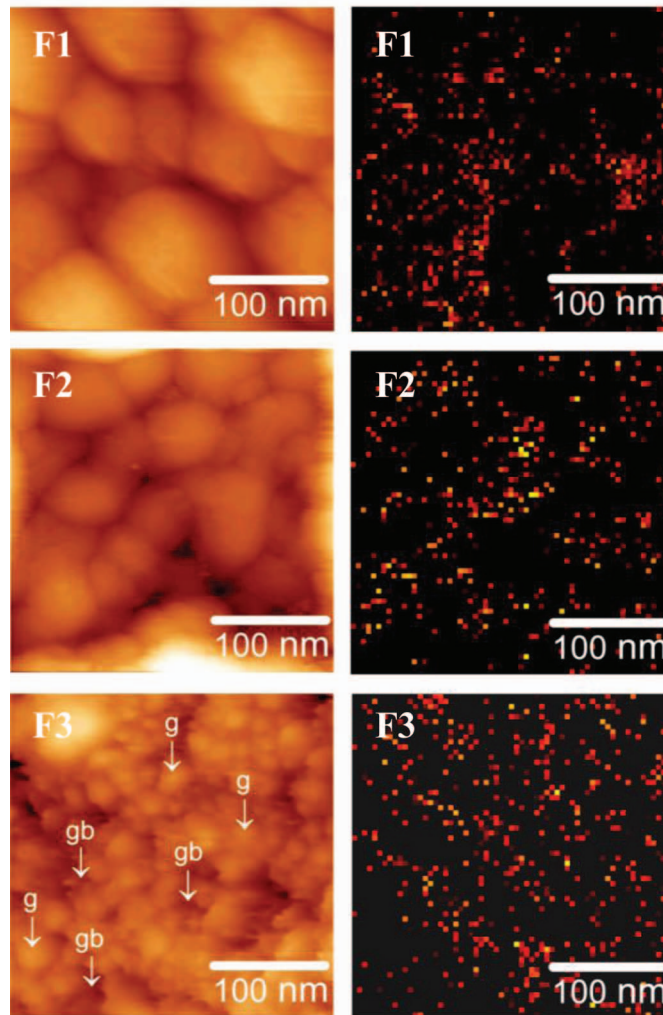


FIG. 6. STM and corresponding CITS images of films F1 (870°C), F2 (700°C) and F3 (600°C) revealing the enhanced surface conductivity of F3 in comparison with films F1 and F2.

to the film surface F1, while it increases for films F2 and F3. This change of the G band intensity is an indication of sliding-induced amorphization/graphitization which can be an important factor to reduce the friction coefficient of these films. Consequently, low and ultra low friction coefficients are measured in the presence of large amount of sp^2 bonding which is evident from the Raman spectra of F2 and F3 films. In each case, the friction coefficient decreases with increase in normal load while the wear rate is found to increase. This may be related to partial transformation of sp^3 diamond material to graphitic sp^2 phase which is higher at higher loads and by higher initial sp^2 carbon fraction. As a result the friction coefficient decreases but the wear rate increases due to the lack of the harder diamond phase.²⁵ It is well-known that the lubricity of graphite and graphitized carbon is due to the sheet-like structure where the intra-planar carbon atoms are covalently bonded through sp^2 bonds while weak van der Waals forces hold these adjacent basal planes together.^{26,27} This allows easy shearing of the planes under various sliding contacts. On the other hand, high wear resistance is caused by the presence of sp^3 diamond in the films. The Raman spectra show that the band intensity and peak position of the fundamental diamond line D^* at $1328\text{--}1332\text{ cm}^{-1}$ is comparable on the surface and in the wear tracks which indicates the stability of the diamond phase during the tribo-induced sliding (Figure 11). The presence of the diamond phase also causes reduction of the friction of the sliding surfaces. A weak TPA peak at 1168 cm^{-1} is observed for

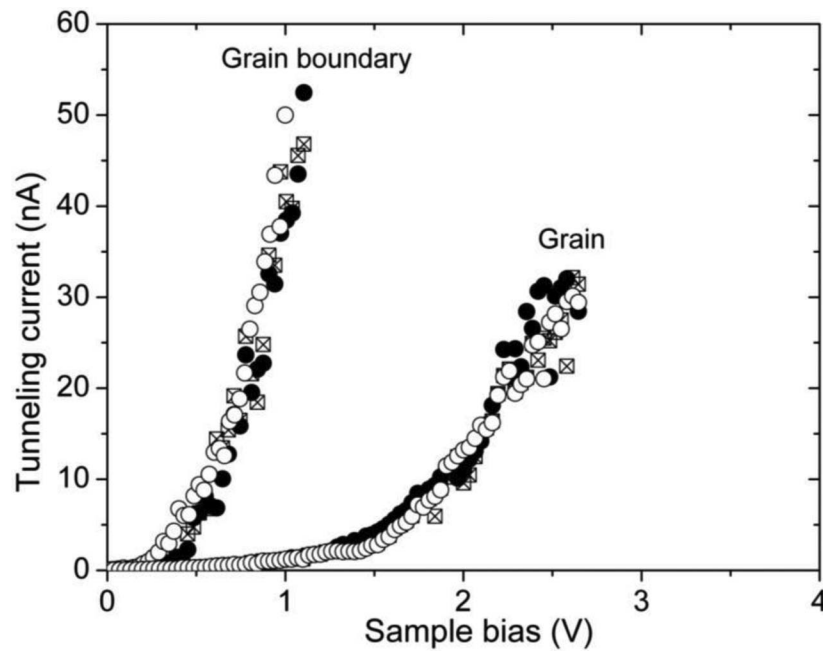


FIG. 7. Typical I-V curves of film F3 obtained from the grains and grain boundaries. Three curves were measured on grains “g” and grain boundaries “gb” at locations marked with arrows in Figure 6.

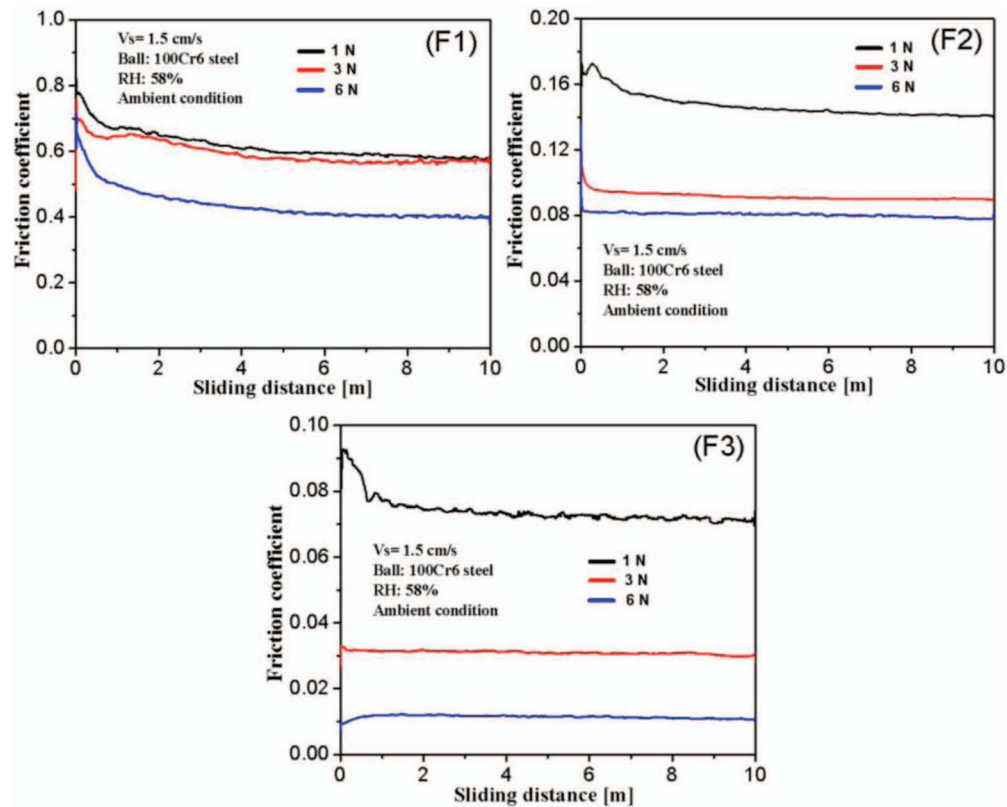


FIG. 8. Friction coefficients of films F1 (870°C), F2 (700°C) and F3 (600°C).

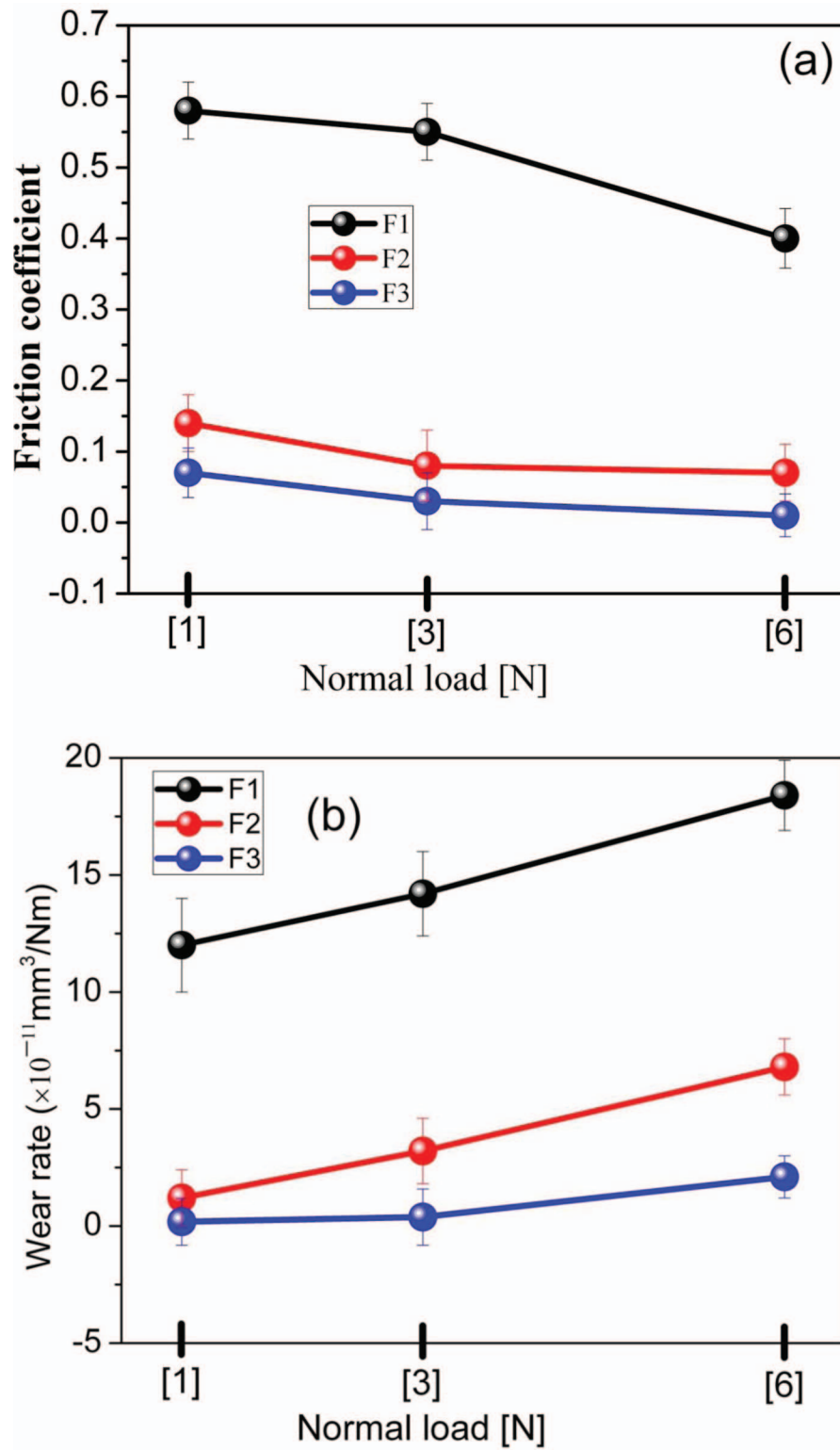


FIG. 9. Comparison of (a) friction coefficients and (b) wear rates at various normal loads plotted with error bars.

TABLE II. Friction coefficient and wear rate of F1, F2 and F3 films as a function of the normal load.

	Friction coefficient			Wear coefficient ($\times 10^{-11}$ mm ³ /Nm)		
	Normal load (N)			Normal load (N)		
	1	3	6	1	3	6
(F1)	0.58	0.55	0.4	120	142	184
(F2)	0.14	0.1	0.08	12	32	68
(F3)	0.07	0.03	0.01	1.8	3.8	21

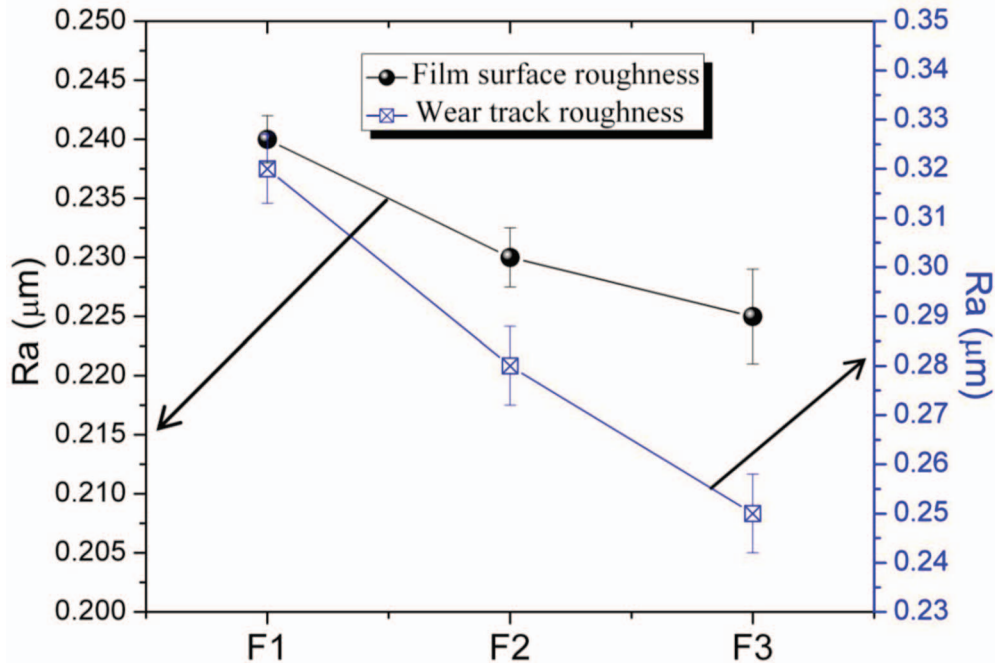


FIG. 10. Surface roughness and wear track roughness of films F1, F2 and F3.

films F2 and F3 which stems from the grain boundary material and conforms a signature of NCD films (Figure 11).

For all films, the silicon peak at 520 cm^{-1} is observed in both spectra. Its band intensity outside the wear track increases from F1 to F3 as it is related with the film thickness and deposition temperature, which decrease from F1 to F3. The second order silicon peak at $944\text{--}948\text{ cm}^{-1}$ appears in the wear track of F1 films. This may be due to the high wear rate of this film which may reduce the film thickness inside the track considerably or even expose the silicon surface. No oxide formation was detected in the wear tracks of all films as evident by Raman spectroscopy (Figure 11). The unworn ball surface also does not show evidence of metallic oxide related features as depicted in Figure 12. However, oxide-related peaks, such as $\alpha\text{-Fe}_2\text{O}_3$ at 656 cm^{-1} and 796 cm^{-1} appear on the sliding surface of the balls in the cases of films F1 and F2, respectively (Figure 12). As steel balls have been used for the wear experiments, this result is not surprising. The metallic oxide peaks are found to be prominent in the Raman spectrum of film F1. This may be one of the primary reasons for the high friction coefficient.¹⁵ The formation of oxide scales on the steel counterbody sliding with ultrananocrystalline diamonds films and its significance on their tribological properties has been studied.²⁸ All three spectra from the balls show peaks which can be related to the film material, among them the fundamental diamond line D* and the G peak indicating the formation of a transfer layer in all three cases. The intensity of diamond line is most prominent for the ball used for film F3, which also contains a broad G peak without any signature of oxides. This spectrum closely resembles those obtained from the surface and the wear track of the film. The formation of

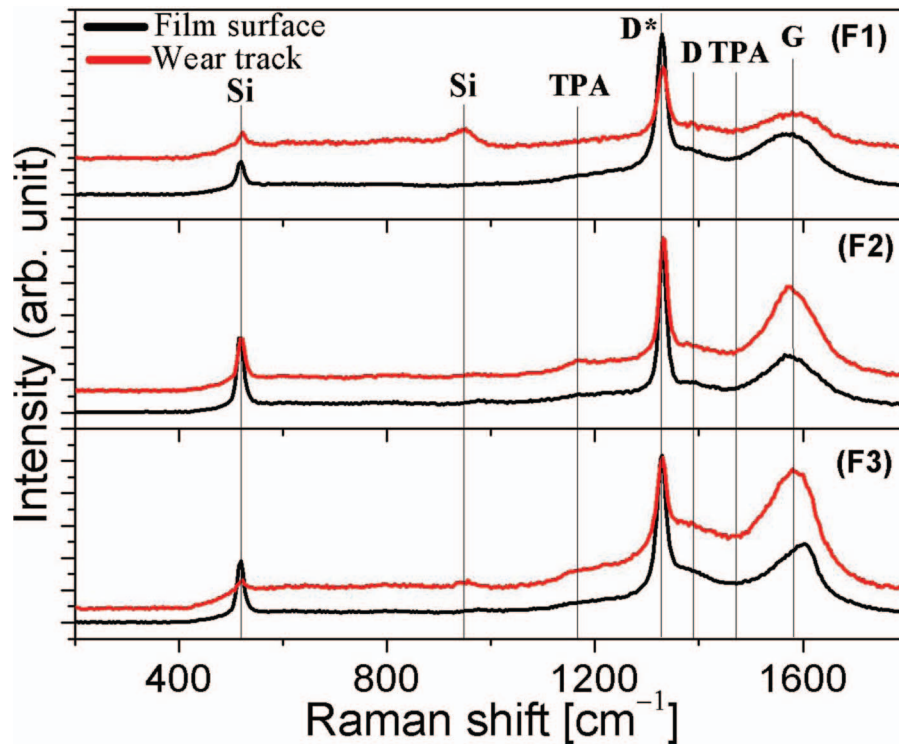


FIG. 11. Micro-Raman spectra from the surface and the wear tracks of the films F1, F2 and F3 obtained at constant load of 3 N.

a carbonaceous transfer layer on the ball, followed by a reduction in friction coefficient has been studied by several authors.^{28–30}

The friction coefficient is found to decrease with increase in normal load as shown in Figure 8. As diamond undergoes plasticity induced amorphization/graphitization, the extent of phase transformation is expected to increase with the applied load.³¹ At high normal loads, more asperities appear and the materials come into more intimate contact. As a consequence, the thickness of the transfer layer increases.³² To investigate this phenomenon on the nanocrystalline diamond films, micro-Raman experiments have been performed inside the wear track of film F2 at different loading conditions of 1 N, 3 N and 6 N as shown in Figure 13. It is clearly seen that the intensity of the G band increases with the normal load which indicates that the surface becomes more amorphous. Enhanced amorphization/graphitization of carbon reduces the shear resistance and hence lowers the friction coefficient. Thus the low friction coefficient at high loads can be attributed to the formation of a continuous lubricating amorphous carbonaceous layer. A transfer layer is observed by the formation of an amorphous/graphitic layer at high loads leading to a reduction of the friction coefficient.^{26,27} One of the basic mechanisms to reduce the friction coefficient of carbon materials is the passivation of the dangling bonds which occurs due to dissociation of water to H- and OH-groups.³³ The behavior of the friction coefficient and the wear rate is directly correlated to the chemical state as well as the surface morphology of the film.

Surfaces with a high roughness essentially have high wear rates. In addition, the increase of the friction coefficient with the surface roughness is well-known fact.²² Films with high hardness and high elastic modulus are indicative of high wear rate if the friction coefficient is high where adhesive and abrasive wear mechanism dominates. High wear rate can also be related to the structural properties of the films. With increase of the amorphous sp^2 phase fractions, wear rate is found to decrease due to low friction coefficient. The images of the wear tracks of all three films obtained at 3 N load are shown in Figure 14. The wear of the corresponding balls is also shown in the inset of the corresponding images. High wear rate causes deformation of the film surface and of the ball

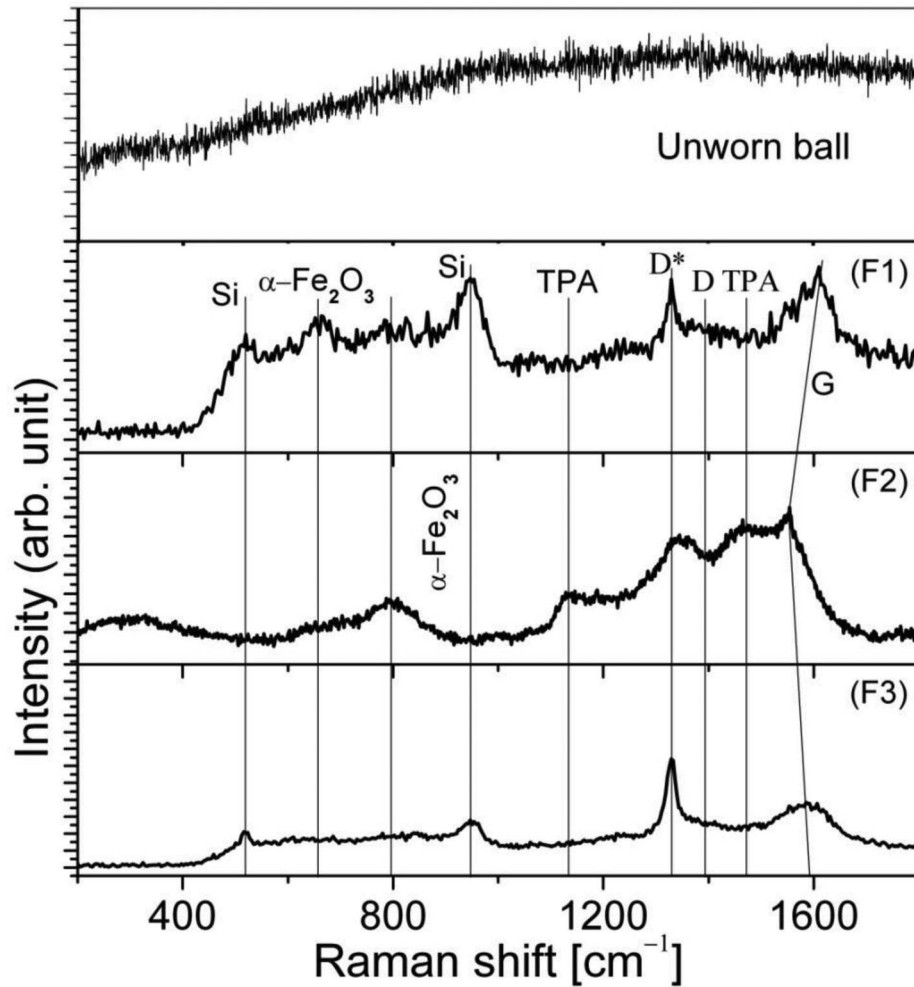


FIG. 12. Micro-Raman spectra from the steel balls after sliding on films F1, F2 and F3 at constant load of 3 N.

counterface as well, as seen in Figure 12(F1), where grooves, cracks and oxide scales are clearly visible. However, the film surface and the ball counterface are found to be less deformed for the films containing higher amorphous sp^2 phase fraction [Figure 12(F2)] and [Figure 12(F3)]. The wear track width is found to decrease from F1 to F3 film. The carbonaceous transfer layer revealed by Raman spectroscopy on the ball counterface further prevents the wear.

IV. CONCLUSIONS

Nanocrystalline diamond films were prepared on silicon substrates by hot filament chemical vapor deposition from CH_4/H_2 mixtures with 1% methane at three different substrate temperatures. With decreasing the substrate temperature, the grain size decreases which causes lower hardness and lower elastic modulus of the films. XPS measurements revealed that the amorphous sp^2 phase fraction increases with decreasing the substrate temperature leading to the change in microstructural properties and increase of surface conductivity. These changes have a prominent effect on friction and wear resistance. The increase of amorphous sp^2 phase fraction results in ultra low friction coefficient. The chemical nature of the surface of the films, wear tracks and ball counterbodies studied by micro-Raman spectra are well-correlated with the friction coefficient and wear resistance. Amorphization of the wear track is found to increase with the applied normal load.

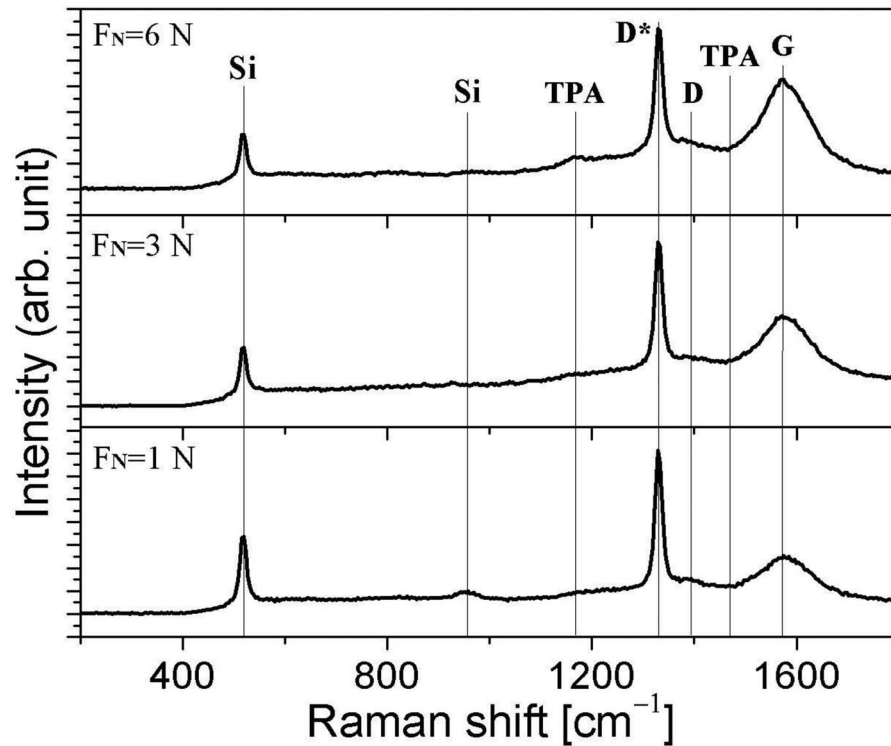


FIG. 13. Micro-Raman spectra of wear tracks formed on film F2 at normal loads of 1, 3 and 6 N.

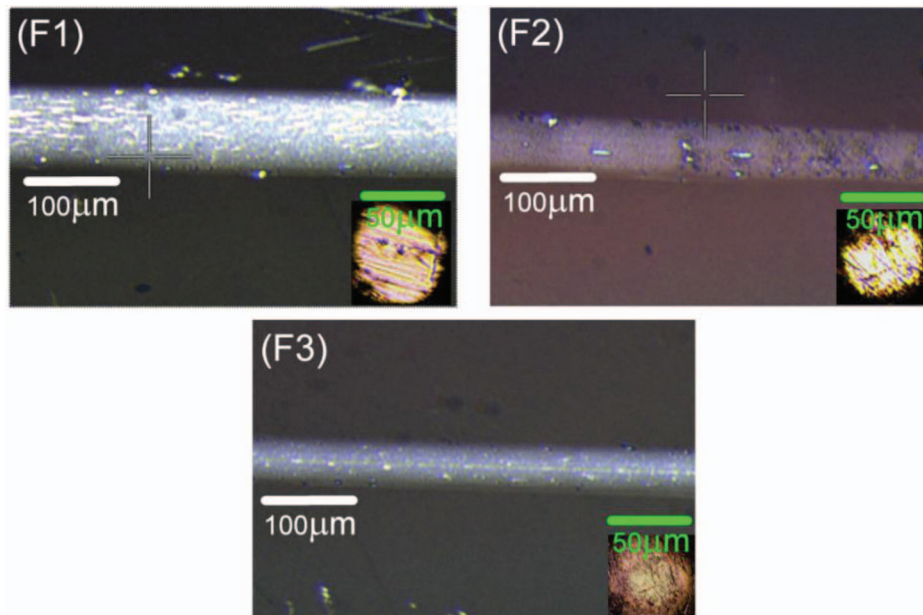


FIG. 14. Optical images of the wear tracks obtained at 3 N normal loads on F1, F2 and F3 specimen and insets showing the corresponding microscopic images of worn balls.

ACKNOWLEDGMENT

The authors would like to thank Dr. S. Dhara for the micro-Raman measurements. Mr. Nanda Gopala Krishna is acknowledged for the XPS measurements. The authors also thank Dr. C.S. Sundar, Director of MSG/IGCAR, for his consistent encouragement and support.

- ¹T. Irifune, A. Kurio, S. Sakamoto, T. Inoue, and H. Sumiya, *Nature* **421**, 599 (2003).
- ²V. Blank, M. Popov, G. Pivovarov, N. Lvova, K. Gogolinsky, and V. Reshetov, *Diamond and Related Materials* **7**, 427 (1998).
- ³C. A. Brookes and E. J. Brookes, *Diamond and Related Materials* **1**, 13 (1993).
- ⁴P. W. May, *Phil. Trans. R. Soc. Lond. A* **358**, 473 (2000).
- ⁵W. Kulisch, *Springer Tracts on Modern Physics*, Heidelberg Berlin (1999).
- ⁶S. Y. Luoa, J. K. Kuo, B. Yeh, J. C. Sung, C. W. Dai, and T. J. Tsai, *Materials Chemistry and Physics* **72**, 133 (2001).
- ⁷Q. P. Wei, Z. M. Yu, L. Ma, D. F. Yin, and J. Yea, *Applied Surface Science* **256**, 1322 (2009).
- ⁸A. R. Konicek, D. S. Grierson, P. U. P. A. Gilbert, W. G. Sawyer, A. V. Sumant, and R. W. Carpick, *Physical Review Letters* **100**, 235502 (2008).
- ⁹F. R. Kloss, M. Najam-Ul-Haq, M. Rainer, R. Gassner, G. Lepperdinger, C. W. Huck, G. Bonn, F. Klauser, X. Liu, N. Memmel, E. Bertel, J. A. Garrido, and D. Steinmuller-Nethl, *Journal of Nanoscience and Nanotechnology* **7**, 4581 (2007).
- ¹⁰X. Liu, F. Klauser, N. Memmel, E. Bertel, T. Pichler, M. Knupfer, A. Kromka, and D. Steinmüller-Nethl, *Diamond and Related Materials* **16**, 1463 (2007).
- ¹¹A. R. Krauss, O. Auciello, D. M. Gruen, A. Jayatissa, A. Sumant, J. Tucek, D. C. Mancini, N. Moldovan, A. Erdemir, D. Ersoy, M. N. Gardos, H. G. Busmann, E. M. Meyer, and M. Q. Ding, *Diamond and Related Materials* **10**, 1952 (2001).
- ¹²P. Hollman, O. Wanstrand, and S. Hogmark, *Diamond and Related Materials* **7**, 1471 (1998).
- ¹³L. Pastewka, S. Moser, P. Gumbsch, and M. Moseler, *Nature Materials* **10**, 34 (2011).
- ¹⁴S. E. Grillo, J. E. Field, and F. M. van Bouwelen, *Journal of Physics D: Applied Physics* **33**, 985 (2000).
- ¹⁵I. P. Hayward, *Wear* **215**, 157 (1992).
- ¹⁶D. S. Grierson and R. W. Carpick, *Nanotoday* **2**, 12 (2007).
- ¹⁷S. Yang, Z. He, Q. Li, D. Zhu, and J. Gong, *Diamond and Related Materials* **17**, 2075 (2008).
- ¹⁸W. Kulisch, C. Popov, T. Sasaki, L. Sirghi, H. Rauscher, F. Rossi, and J. P. Reithmaier, *Physica Status Solidi* **208**, 70 (2011).
- ¹⁹W. C. Oliver and G. M. Pharr, *Journal of Materials Research* **7**, 1564 (1992).
- ²⁰R. Kuschneril, P. Hess, D. Alberl, and W. Kulisch, *Thin Solid Films* **312**, 66 (1998).
- ²¹E. Salgueiredo, M. Amaral, M. A. Neto, A. J. S. Fernandes, F. J. Oliveira, and R. F. Silva, *Vacuum* **85**, 701 (2011).
- ²²W. Kulisch, C. Popov, S. Boycheva, M. Jelinek, P. N. Gibson, and V. Vorliceck, *Surface and Coatings Technology* **200**, 4731 (2006).
- ²³V. Janos, *Surface Science* **563**, 183 (2004).
- ²⁴K. Panda, B. Sundaravel, B. K. Panigrahi, P. Magudapathy, D. N. Krishna, K. G. M. Nair, H. C. Chen, and I-N. Lin, *Journal of Applied Physics* **110**, 44304 (2011).
- ²⁵D. C. Barbosa, F. A. Almeida, R. F. Silva, N. G. Ferreira, V. J. Trava-Airoldi, and E. J. Corat, *Diamond and Related Materials* **18**, 1283 (2009).
- ²⁶A. Erdemir, G. R. Fenske, A. R. Krauss, D. M. Gruen, T. McCouley, and R. T. Csencsits, *Surface and Coatings Technology* **120–121**, 565 (1999).
- ²⁷J. Lancaster and J. Pritchard, *Journal of Physics D: Applied Physics* **13**, 1551 (1980).
- ²⁸N. Kumar, Neha Sharma, S. Dash, C. Popov, W. Kulisch, J. P. Reithmaier, G. Favaro, A. K. Tyagi, and Baldev Raj, *Tribology International* **44**, 2042 (2011).
- ²⁹H. Zajdi, D. Paulmier, and J. Lepage, *Applied Surface Science* **44**, 221 (1990).
- ³⁰R. Polini, M. Barletta, and G. Cristofanilli, *Thin Solid Films* **519**, 1629 (2010).
- ³¹B. Lichun, Z. Guangan, L. Zhibin, W. Zhiguo, W. Yunfeng, W. Liping, and Y. Pengxun, *Journal of Applied Physics* **110**, 33521 (2011).
- ³²E. H. Lee, D. M. Hembree, Jr., G. R. Rao, and L. K. Mansur, *Physical Review B* **48**, 15540 (1993).
- ³³A. R. Konicek, D. S. Grierson, A. V. Sumant, T. A. Friedmann, J. P. Sullivan, P. U. P. A. Gilbert, W. G. Sawyer, and R. W. Carpick, *Physical Review B* **85**, 155448 (2012).